

## The transcription factors MYB80 and TEK coordinate callose wall degradation and pollen exine formation in *Arabidopsis*

Xiaofeng Xu,<sup>1,\*</sup> Kaiqi Wang,<sup>2,†</sup> Yahui Yu,<sup>2,†</sup> Xin Zhao,<sup>1</sup> Yuyi Guo,<sup>1</sup> Yaqi Liu,<sup>1</sup> Xuexue Qian,<sup>1</sup> Naiying Yang,<sup>1</sup> Ping Xu,<sup>1</sup> Zhong-Nan Yang<sup>1,\*</sup>

<sup>1</sup>Shanghai Collaborative Innovation Center of Plant Germplasm Resources Development, College of Life Sciences, Shanghai Normal University, Shanghai 200234, China

<sup>2</sup>College of Biological and Environmental Engineering, Jingdezhen University, Jiangxi 333000, China

\*Author for correspondence: [xiaofengxu@shnu.edu.cn](mailto:xiaofengxu@shnu.edu.cn) (X.X.) and [znyang@shnu.edu.cn](mailto:znyang@shnu.edu.cn) (Z.-N.Y.)

†These authors contributed equally to this work.

The author responsible for distribution of materials integral to the findings presented in this article in accordance with the policy described in the Instructions for Authors (<https://academic.oup.com/plphys/pages/General-Instructions>) is Xiaofeng Xu ([xiaofengxu@shnu.edu.cn](mailto:xiaofengxu@shnu.edu.cn)).

### Abstract

Pollen development involves cell wall alteration of the male gametophyte, which is critical for plant fertility and requires MYB80 and TRANSPOSABLE ELEMENT SILENCING VIA AT-HOOK (TEK) transcription factors in *Arabidopsis* (*Arabidopsis thaliana*). In this study, we found that the *myb80 tek* double mutant exhibits a compromised degradation of the tetrad callose wall and downregulation of 5 ANTHHER-SPECIFIC PROTEIN 6 (A6) genes encoding  $\beta$ -1,3-glucanase. The quintuple mutant of A6 (*a6-quint*) exhibited delayed callose wall degradation and defective exine structure, and its pollen had a weakened UV resistance. The quadruple mutant of A6 (*a6-quad*) restored the fertility of *rums-2*, a thermosensitive genic male sterile (TGMS) line where the transition from tetrad wall to pollen wall is defective. Transgenic expression of A6 and A6.2 driven by the A9 promoter led to the expression of the 2 genes in the tapetum at earlier anther developmental stages, which caused premature callose wall dissolution and impeded exine formation, indicating the importance of the temporal control of A6s. Furthermore, dual-luciferase and ChIP assay results confirmed the direct regulation of MYB80 and TEK in activating the expression of the above A6s in the tapetum. In conclusion, callose degradation mediated by the MYB80/TEK-A6 pathway is required for the transition from tetrad callose wall to pollen wall.

### Introduction

Meiosis occurs during the maturation of germ cells in both animals and plants. In plants, formation of male reproductive cells via meiosis is accompanied by dynamic deposition and disassembly of the tetrad wall (Sanders et al. 1999; Scott et al. 2004). The tetrad wall consists of the inner callose wall and the outer primary wall which is composed of cellulose and pectin. The callose wall is dense and encases 4 haploid microspores as their protective barrier (Heslop-Harrison 1968; Scott et al. 2004; Shi et al. 2015; Wang et al. 2022). It provides the scaffold for primexine formation, which precedes and is essential for the development of species-specific pollen exine (Ariizumi and Toriyama 2011; Radja et al. 2019). As the exine of each microspore forms, the callose wall is dissembled and dissolved. This allows the microspores to be released from the tetrad and further mature in the locule (Blackmore et al. 2007). In conclusion, the deposition and dissolution dynamics of the tetrad callose wall are pivotal factors in pollen development.

The deposition of  $\beta$ -1,3-glucans between the microspore plasma membrane and the primary wall of pollen mother cell forms a specialized polysaccharide matrix, which is known as the tetrad callose wall (Dong et al. 2005; Nishikawa et al. 2005; Ariizumi and Toriyama 2011; Radja et al. 2019). In *Arabidopsis* (*Arabidopsis thaliana*), several callose synthases (CalS) play crucial roles in callose

biosynthesis during callose wall development (Dong et al. 2005; Enns et al. 2005; Toller et al. 2008; Huang et al. 2013). On the other hand, the callose wall is progressively dissolved after meiosis by callase for microspore release. Callase is a mixture of enzymes that are secreted from the tapetum, with the main component being  $\beta$ -1,3-glucanase (Frankel et al. 1969; Stieglitz and Stern 1973; Worrall et al. 1992; Hird et al. 1993; Scott et al. 2004; Blackmore et al. 2007). To date, a few genes encoding anther-specific  $\beta$ -1,3-glucanase have been identified in plants. Aberrant expression of these genes results in abnormal degradation of the callose wall that affects normal pollen development (Izhar and Frankel 1971; Worrall et al. 1992; Winiarczyk et al. 2012; Liu et al. 2017). Mis-expression of  $\beta$ -1,3-glucanase at an earlier stage results in the premature dissolution of callose and pollen collapse in tobacco (*Nicotiana tabacum*) (Worrall et al. 1992), while silencing of rice (*Oryza sativa*) *Oryza sativa glucanase 1* (*Osg1*) in anther delays callose dissolution and affects pollen maturation (Wan et al. 2011). Hence, the timely callose dissolution of tetrad wall involving  $\beta$ -1,3-glucanase is required for normal pollen development in both monocot and dicot plants, but the spatiotemporal regulation of the expression of callase remains unclear.

The mixed enzymes of callase are produced and secreted from the tapetum. The tapetum is the innermost layer of secretory cells in the anther. Dysfunction of the tapetum directly leads to

Received September 6, 2024. Accepted February 2, 2025.

© The Author(s) 2025. Published by Oxford University Press on behalf of American Society of Plant Biologists. All rights reserved. For commercial re-use, please contact [reprints@oup.com](mailto:reprints@oup.com) for reprints and translation rights for reprints. All other permissions can be obtained through our RightsLink service via the Permissions link on the article page on our site—for further information please contact [journals.permissions@oup.com](mailto:journals.permissions@oup.com).

abnormal pollen development and/or male sterility (Lu et al. 2014; Liu et al. 2017; Li et al. 2017b). In *Arabidopsis*, the DYSFUNCTIONAL TAPETUM1 (DYT1)–DEFECTIVE IN TAPETAL DEVELOPMENT AND FUNCTION 1 (TDF1)–ABORTED MICROSPORE (AMS) transcriptional regulatory pathway controls the development and function of tapetum including the callose wall dissolution of tetrad (Zhang et al. 2006; Yang et al. 2007; Zhang et al. 2007; Zhu et al. 2008, 2011; Tidy et al. 2022). Microspore development depends on the deposition and dissolution of callose wall, the prerequisite for the formation of exine with complex composition of sexine and nexine. MYB80, also known as MYB103/MALE STERILE 18 (MYB103/MS188), encodes an R2R3 MYB transcription factor that specially affects sexine formation (Zhang et al. 2007). TRANSPOSABLE ELEMENT SILENCING VIA AT-HOOK (TEK) encodes an AT-hook family protein that functions as a nuclear transcription factor determining nexine formation (Lou et al. 2014). AMS was found to control the formation of exine by regulating MYB80 and TEK expression in the tapetum to control sexine and nexine formation, respectively (Lou et al. 2014; Jia et al. 2015; Xiong et al. 2016; Wang et al. 2018). Despite the apparent relationship between the callose wall and exine formation, it is unknown if MYB80 and TEK regulate callose dissolution by regulating callase transcription.

In *Arabidopsis* and *Brassica napus*, ANTHHER-SPECIFIC PROTEIN 6 (A6) encodes an anther-specific  $\beta$ -1,3-glucanase involved in callose degradation. A6 is secreted from the tapetum into the locule (Hird et al. 1993; Wang et al. 2022). In the present study, we further confirm the function of A6 family in pollen development by obtaining and analyzing the quintuple mutant of A6 (*a6-quint*). In addition, *in vitro* and *in vivo* biochemical investigations are carried out to understand the role of MYB80 and TEK in regulating the expression of all 5 A6 members in the tapetum, and a control model for the transition from callose wall to pollen wall is proposed.

## Results

### Callose degradation on tetrad wall is substantially delayed in the *myb80 tek* anther

It is known that AMS regulates the expression of MYB80 and TEK in the tapetum during tetrad stage (Zhang et al. 2007; Lou et al. 2014). To understand their roles in tetrad wall and exine remodeling, we generated *myb80 tek* double mutant. Transmission electron microscopy (TEM) was used to observe the exine composition of *myb80 tek* and wild-type (WT) microspores, and semithin sections of *ams*, *myb80*, *tek*, and *myb80 tek* anthers were also stained with toluidine blue (Fig. 1A) and aniline blue (Fig. 1B), respectively, for the observation of callose deposition and dissolution during the pollen development. In agreement with our previous findings (Zhang et al. 2007; Lou et al. 2014), the sexine and nexine layers were completely absent on the surface of *myb80 tek* microspore, when the well-defined exine structure could be observed in WT (Supplementary Fig. S1). Further analysis from toluidine and aniline blue staining revealed that the callose wall surrounding tetrads degenerates and individual microspores released at anther Stage 8 in WT. However, the callose remained visible, and the microspores were not released from the tetrads until Stage 11 in *myb80 tek* anthers (Fig. 1, A and B), indicating the essential role of MYB80 and TEK in regulating callose wall degradation. This is similar to the anther development of *ams*, where the callose remained visible after Stage 7 (Fig. 1, A and B). In a single mutant of *myb80*, callose deposition in tetrad wall was normal, but callose dissolution was incomplete even at Stage 10 (Fig. 1, A and B),

indicating the requirement of MYB80 in callose dissolution after Stage 7. In *tek*, microspores were completely released from tetrads, and no callose was detected in its anther after Stage 7 (Fig. 1, A and B), suggesting that loss of function of TEK alone does not affect callose degradation. However, similar to *ams*, a further delay in callose degradation was observed in *myb80 tek* compared to WT, *myb80*, and *tek* mutants. The fine tetrad structure and callose fluorescence were clearly observed at Stages 10 to 11 of *myb80 tek* anthers while their tapetal cells were vacuolated at Stages 7 to 10. These results indicate the importance of combined expression of MYB80 and TEK in controlling the timing of callose degradation. Therefore, AMS may act through MYB80 and TEK to regulate the callose degradation during microspore development.

### A6 and its homologs participate in degrading tetrad callose

Tapetal cells are essential for tetrad callose degradation in the anther. A6, the anther-specific  $\beta$ -1,3-glucanase is thought to be involved in this process (Hird et al. 1993; Shi et al. 2015). To confirm it, we obtained the homozygous T-DNA insertion mutant *a6* (Supplementary Fig. S2). The *a6* mutant exhibited a minor defect on callose degradation (Fig. 2D; Supplementary Fig. S2), which could be caused by gene redundancy. Hence, we further searched and identified 48 homologs of A6 in *Arabidopsis* (Supplementary Fig. S3). Among these, 17 members were found to be expressed in the tapetum (Supplementary Fig. S4) based on the published transcriptome data of *Arabidopsis* (Li et al. 2017a). To further identify the putative A6 members that may play a role in callose degradation, we examined the expression levels of these 17 genes in the *ams* inflorescence using RT-qPCR analysis as *ams* exhibit defective callose degradation (Fig. 1B). The results showed downregulation (fold change [FC] < 0.5;  $P < 0.05$ ) of 5 A6 homologs (A6, A6.2, A6.3, A6.4, and A6.5) (Fig. 2A; Supplementary Fig. S5). The downregulation of these 5 genes also occurred in the inflorescence of *myb80 tek* (Fig. 2A), while A6, A6.2, and A6.5 were downregulated in *myb80* and A6.2 and A6.5 in *tek* mutants (Fig. 2B). These results suggest that the expression of A6 homologs in the tapetum is coordinately regulated by MYB80 and TEK.

To further understand their function in callose degradation, we obtained T-DNA mutation lines of other 4 A6 members from the *Arabidopsis* Biological Resource Center (ABRC) (<http://abrc.osu.edu>). The single, double (*a6 a6.2*), and triple (*a6 a6.2 a6.3*) mutants were fully fertile (Supplementary Fig. S2) and showed no obvious defects in callose wall degradation. It was the quintuple mutant of *a6 a6.2 a6.3 a6.4 a6.5* (*a6-quint*) that showed a noticeably delayed callose degradation (Fig. 2C; Supplementary Fig. S2). In WT, the callose fluorescence disappeared in the anther at Stage 8, but callose was detectable in *a6-quint* at Stage 9 (Fig. 2C). Subsequent statistical analysis revealed that tetrad callose degradation was significantly delayed in the *a6-quint* mutant compared to WT, *a6*, and *a6-quad* mutants (Fig. 2D; Supplementary Fig. S2). These results suggest the functional redundancy of A6 and its other family members and confirm their importance in the timely degradation of tetrad callose in the anther.

To investigate whether these downregulated A6s in the tapetal cells are responsible for the delayed callose degradation in the *myb80 tek* anther, we generated transgenic plants expressing A6 and A6.2 driven by TEK promoter in *myb80 tek* mutant background, respectively. TEK promoter drives gene expression specifically in the tapetum at Stage 7 during the anther development (Lou et al. 2014). The transgenic *pTEK::A6* (*myb80 tek*) and *pTEK::*

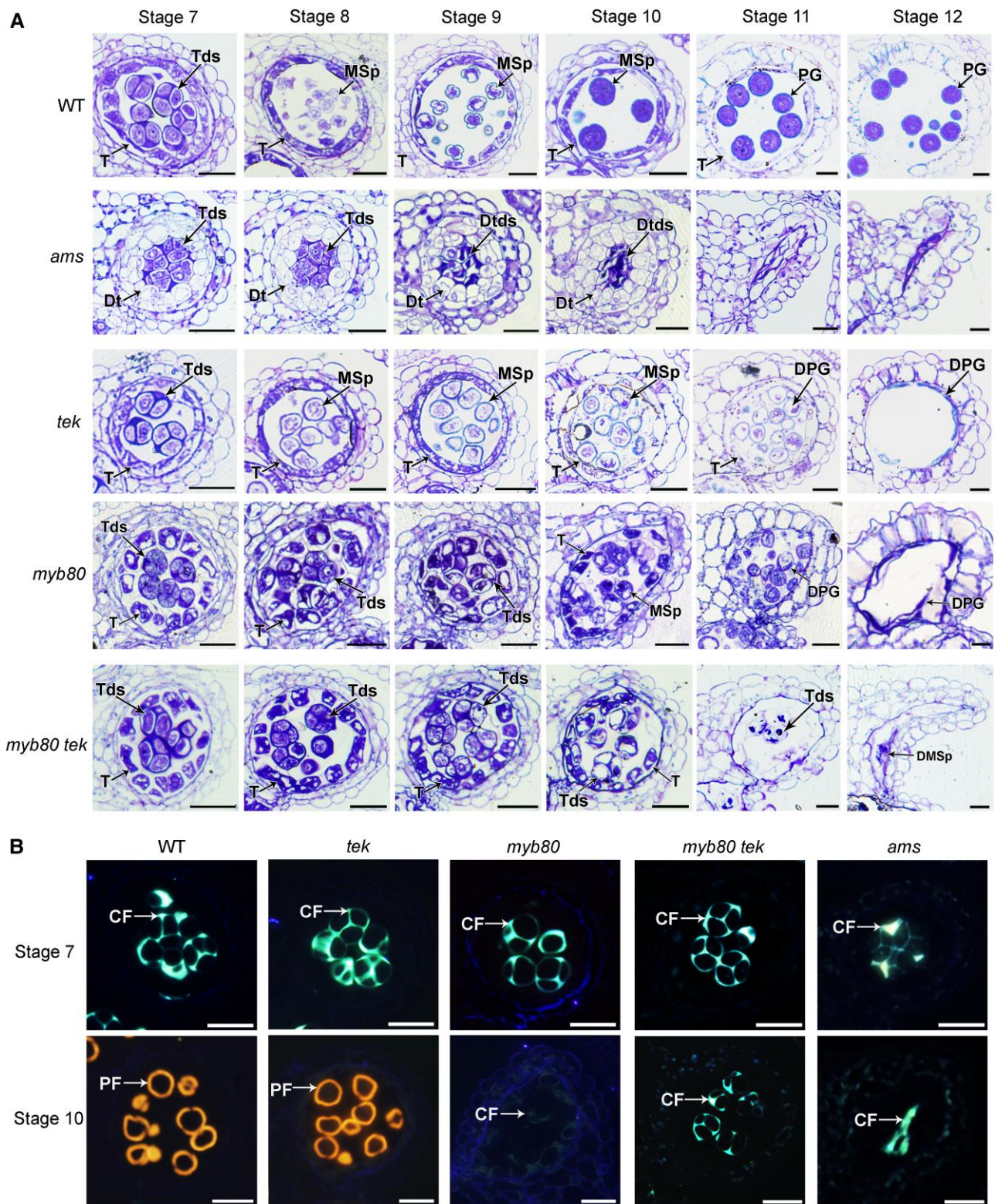


**Figure 1.** Tetrad callose wall degradation is substantially delayed in *myb80 tek* mutant anthers. **A**) Semithin sections of the anthers of the wild-type (WT), *ams*, *tek*, *myb80*, and *myb80 tek* mutants at Stages 7 to 12 of *Arabidopsis* anther development (Sanders et al. 1999). Tapetum development is severely disrupted at early stages in the *ams* anther but slightly impaired in *myb80 tek* anthers. At Stage 11, the tetrads remain in the *myb80 tek* anther but not in the WT, *myb80*, and *tek* anthers. Tds, tetrads; Dtds, degenerated tetrads; PG, pollen grain; DPG, degenerated pollen grain; MSp, microspore; DMSp, degenerated microspore; T, tapetum; Dt, degenerated tapetum. Bars, 20  $\mu$ m. **B**) Aniline blue staining of anther sections of WT, *ams*, *tek*, *myb80*, and *myb80 tek* mutants showing callose degeneration at anther Stages 7 and 10. At Stage 7, the fluorescence of callose (CF) indicates that callose deposition is not altered in these plants. At Stage 10, CF is absent in WT and *tek* anthers, whereas weak CF is found in *myb80* anthers and strong CF can be observed in tetrads of *myb80 tek* anthers and in the locule of *ams* anthers. PF, pollen wall autofluorescence; Bars, 20  $\mu$ m.

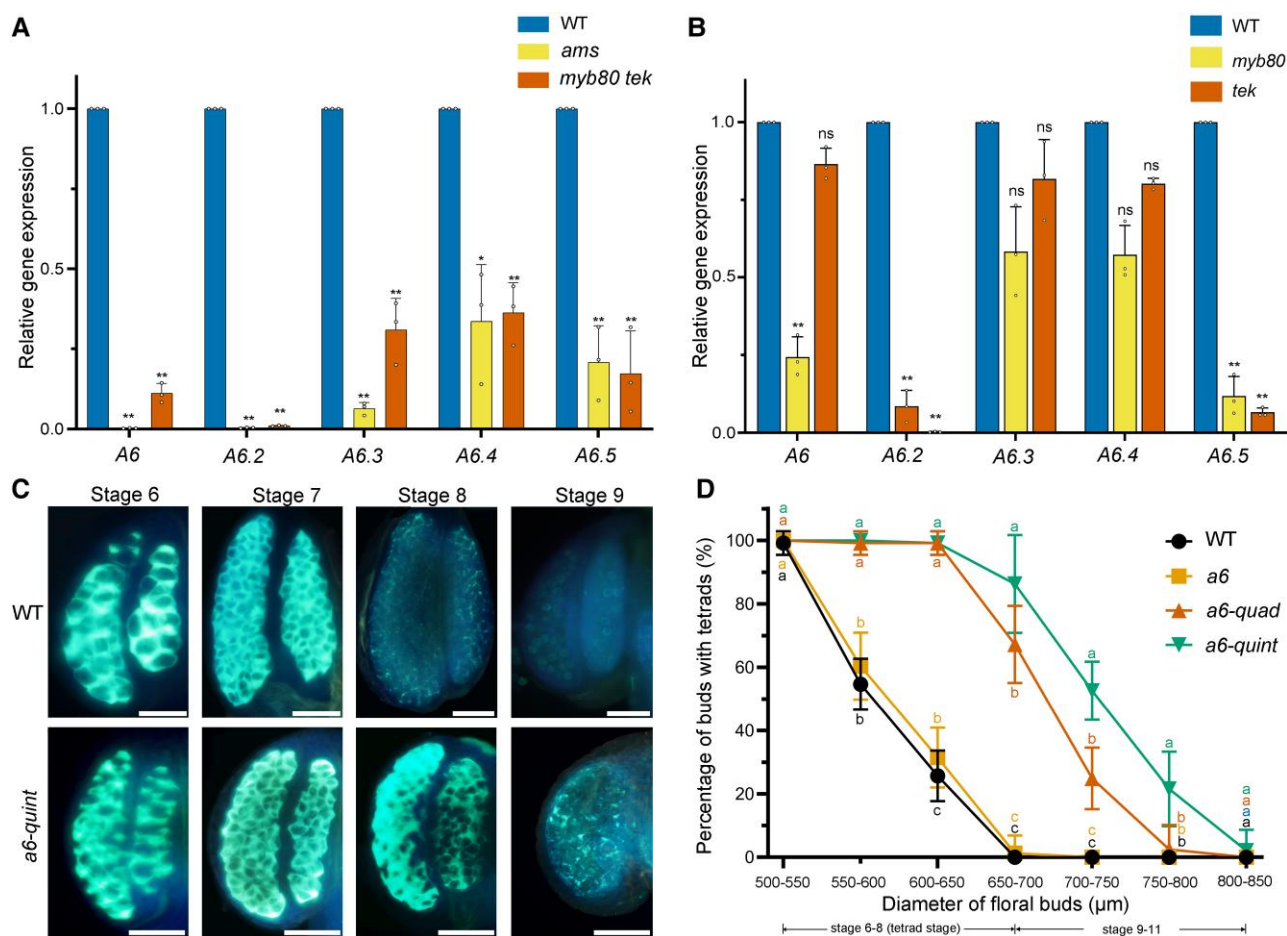


**Figure 2.** A6 and its homologues are involved in tetrad callose degradation. **A to B)** Expression of A6, A6.2, A6.3, A6.4, and A6.5 in flower buds from wild-type (WT), *myb80*, *tek*, *ams*, and *myb80 tek* plants, as determined by RT-qPCR. The expression level was normalized to that of *TUBULIN BETA8* (*TUB*) and compared with the WT samples. Means with error bars indicate SD ( $n=3$ ). A two-tailed t test was used to evaluate the statistical significance difference from the WT value (FC < 0.5, \* $P < 0.05$ , and \*\* $P < 0.01$ ); ns, not significant (FC > 0.5,  $P > 0.05$ ). **C)** Aniline blue staining of the anthers of WT and *a6-quint* (*a6 a6.2 a6.3 a6.4 a6.5*) showing tetrad callose deposition and degradation from anther Stages 6 to 9. In WT, the tetrad callose rapidly dissolved after Stage 7 and was not observed in anthers at Stage 9. In *a6-quint* anthers, the callose staining remained observable at Stage 9, indicating incomplete callose degradation. Bars, 50  $\mu\text{m}$ . **D)** The rate of microspore release from the tetrads in WT, *a6*, *a6-quad* (*a6.2 a6.3 a6.4 a6.5*), and *a6-quint* anthers. The percentage was defined as the number of buds having tetrads divided by the total number of buds. The rate of buds with tetrads decreased dramatically from 550 to 650  $\mu\text{m}$  (bud size) in WT and *a6* mutants; however, tetrad dissolution was slower in the *a6-quad* and *a6-quint* mutants than in the WT. Means with error bars indicate SD ( $n=20$ ). Different letters indicate significant differences using Tukey's multiple comparisons test (one-way ANOVA,  $P < 0.05$ ; Supplementary Data Set 2).

A6.2 (*myb80 tek*) lines showed increased expression of A6 and A6.2 in their inflorescence but remained sterile (Supplementary Fig. S6). Aniline blue staining showed a notable decrease in callose fluorescence in *pTEK::A6 (myb80 tek)* and *pTEK::A6.2 (myb80 tek)* lines at later stages compared to *myb80 tek* (Supplementary Fig. S6). These findings suggest that complementation of A6 and A6.2 in the tapetum can partially restore callose degradation in *myb80 tek*. This provides additional confirmation that regulation of A6s in the tapetum by MYB80 and TEK is part of the mechanism underlying the tetrad callose degradation.

### Pollen exine pattern was altered, and UV resistance was compromised in *a6-quint*

Biosynthesis and deposition of callose wall are essential for exine development and male fertility. After the formation of primary exine framework (columella and tectum), the callose wall is dissolved. However, little was known about the effects of callose degradation on exine formation (Scott et al. 2004; Shi et al. 2015;

Radja et al. 2019). Since the *a6-quint* exhibited a significant delay in tetrad callose degradation (Fig. 2), the development of pollen wall was further investigated using TEM. We found that the tetrads were properly formed during early Stage 7 in *a6-quint* anthers, where the haploid microspores were enclosed by the tetrad wall with proper callose deposition. This indicates that callose synthesis is not affected in *a6-quint* (Supplementary Fig. S7). The tetrad stage is ended with the complete callose degradation and the nexine formation, indicating the completion of the transition from Stage 7 to Stage 8 during the anther development (Ariizumi and Toriyama 2011; Lou et al. 2014). In WT, microspore was released when both nexine and sexine were developed at its cell membrane at Stage 8 (Fig. 3A). At Stage 8 of *a6-quint*, continuous nexine layers formed surrounding the microspores but the callose of tetrad wall remained (Fig. 3B). Its pollen grains exhibited aberrant sexine structure with the columella shorter and wider than those in WT (Fig. 3, C to E; Supplementary Fig. S8). In addition, the *a6-quint* pollen grains had smaller lacunae than WT ones and their exine exhibited a distorted reticulate pattern (Supplementary Fig. S8).

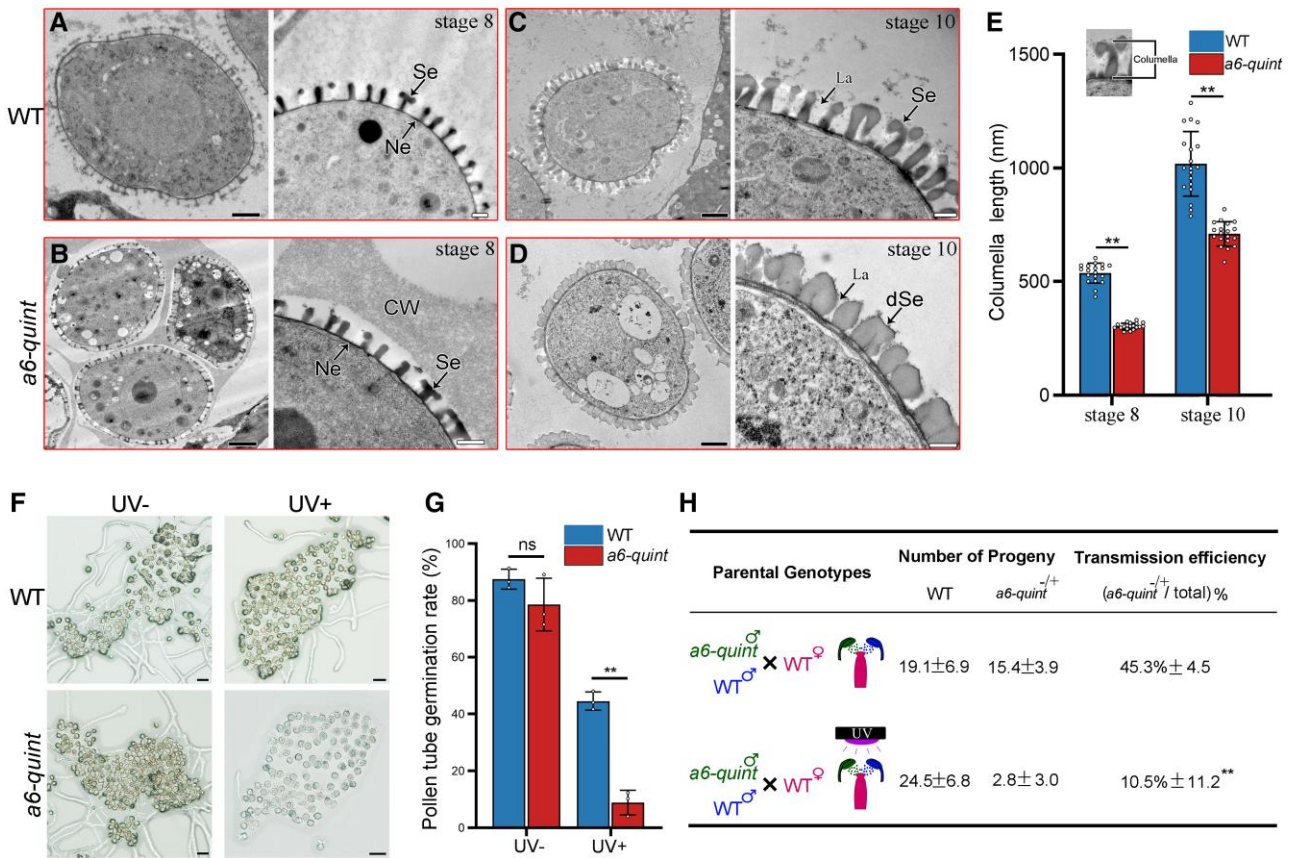


**Figure 3.** The *a6-quint* mutation affects the pollen wall pattern and UV resistance of pollen grain. **A to D)** TEM images of pollen wall structure of wild-type (WT) (A and C) and *a6-quint* (B and D) pollen at Stages 8 and 10. By the time the nexine layer is formed, the callose wall is completely dissolved in WT anthers (A), but the tetrad structure and thick callose wall remain in *a6-quint* anthers (B). At Stage 10, WT pollen shows typical T-shaped sexine and lacuna space (C), whereas *a6-quint* pollen shows defective sexine with restricted lacuna (D). CW, callose wall; Ne, nexine; Se, sexine; La, lacuna; dSe, defective sexine. Black bars, 2,000 nm; white bars, 500 nm. **E)** Statistical analysis of length of the columella of WT and *a6-quint* pollen at Stages 8 and 10. Columella formation is significantly impaired in *a6-quint* mutant pollen. Each point represents the length of columella for WT and *a6-quint* pollen at the examined developmental stage. Means with error bars indicate SD ( $n = 19$ ). A two-tailed t test was used to evaluate statistical significance difference (\*\* $P < 0.01$ ; ns,  $P > 0.05$ ). **F)** Pollen germination of WT and *a6-quint* pollen after the treatment of dark or ultraviolet irradiation (UV) for 5 min. The *a6-quint* pollen has defects in pollen germination under UV conditions. Images were captured under a light microscope at the same magnification. Bars, 50  $\mu\text{m}$ . **G)** The pollen tube germination rate of WT and *a6-quint* pollen after the treatment of dark or UV. The germination of the *a6-quint* pollen was significantly reduced after the UV treatment. Means with error bars indicate SD ( $n = 3$ ). A two-tailed t test was used to evaluate statistical significance difference (\*\* $P < 0.01$ ; ns,  $P > 0.05$ ). **H)** Transmission efficiency of WT and *a6-quint* pollen under normal or UV conditions. Matured pollen grains from WT and *a6-quint* pollen simultaneously spread on the same WT stigma and then treated by UV irradiation for 5 min. Genotypes of  $F_1$  progeny were determined using PCR. Means with error indicate SD ( $n = 20$  siliques). The transmission rate shows that the pollination efficiency of *a6-quint* pollen is similar to that of WT under normal conditions, but the efficiency of *a6-quint* pollen is significantly reduced under UV conditions. A two-tailed t test was used to evaluate statistical significance difference (\*\* $P < 0.01$ ; ns,  $P > 0.05$ ; [Supplementary Data Set 2](#)).

*a6-quint* pollen showed a broader tectum structure than WT, *a6*, *a6-quad*, and other *a6* mutants ([Supplementary Fig. S8](#)). As illustrated in the diagram ([Supplementary Fig. S8](#)), the failed formation of sexine and smaller lacunae may directly result from the delayed degradation of callose in the *a6-quint* mutants due to the loss of function of A6s (A6, A6.2, A6.3, A6.4, and A6.5).

Pollen exine serves as the primary protective shield against various biotic and abiotic stresses. Ultraviolet (UV) irradiation is considered an inevitable type of abiotic stress for pollen grains under natural conditions ([Rozema et al. 2001](#); [Xue et al. 2020](#); [Zhao et al. 2023](#)). The exine of *a6-quint* pollen grains was deformed and pudgy ([Fig. 3D](#); [Supplementary Fig. S8](#)). To investigate whether the abnormal exine affects pollen germination under UV conditions, an in vitro pollen grain germination assay was carried out. The average germination rate of *a6-quint* pollens (78.6%) was similar to that of WT pollens (87.5%) under normal conditions. However, the germination rate of *a6-quint* pollen grains (8.8%) was significantly reduced after UV treatment compared to the WT (44.5%), suggesting a compromised UV tolerance of *a6-quint*

pollen ([Fig. 3, F and G](#)). Furthermore, mature pollen grains from *a6-quint* and WT were applied on the same stigma of WT followed by UV radiation treatment, and the genotypes of the progeny in each silique produced from the pollination were analyzed. Without UV radiation, there were similar average proportions of *a6-quint*<sup>-/+</sup> (45.3%) and WT (54.7%) offsprings. However, only 10.5% of the average offspring proportion were *a6-quint*<sup>-/+</sup>, indicating the significant reduction of successful pollination of *a6-quint* pollens under UV treatment ([Fig. 3H](#)). These findings demonstrate that the abnormal exine pattern in *a6-quint* pollen adversely affects the competitive ability in pollination under UV conditions.

### Delayed callose wall degradation provides additional pollen protection

Our previous research has shown that delayed callose degradation can prevent pollen abortion caused by defective exine in various photo/thermosensitive genic male sterility (P/TGMS)

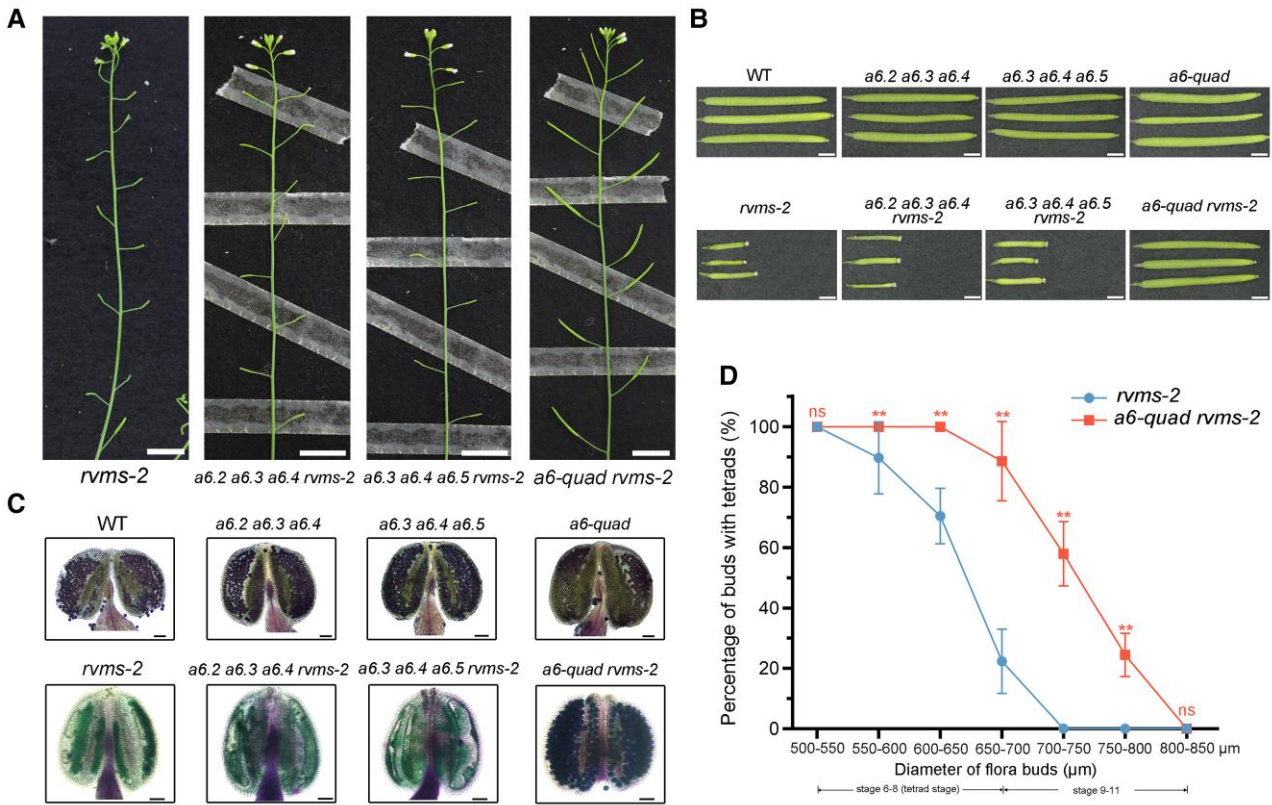


**Figure 4.** Delayed callose degradation facilitates fertility recovery in *rvms-2* mutant. **A)** Phenotypes of *rvms-2*, *a6.2 a6.3 a6.4 rvms-2*, *a6.3 a6.4 a6.5 rvms-2*, and *a6-quad rvms-2* (*a6.2 a6.3 a6.4 a6.5 rvms-2*) mutants. The *rvms-2*, *a6.2 a6.3 a6.4 rvms-2*, and *a6.3 a6.4 a6.5 rvms-2* plants were sterile, but *a6-quad rvms-2* mutant shows normal fertility. Bars, 1 cm. **B)** The silique from wild-type (WT), *rvms-2*, *a6.2 a6.3 a6.4*, *a6.2 a6.3 a6.4 rvms-2*, *a6.3 a6.4 a6.5*, *a6.3 a6.4 a6.5 rvms-2*, *a6-quad*, and *a6-quad rvms-2* mutants. The short siliques in *rvms-2*, *a6.2 a6.3 a6.4 rvms-2*, and *a6.3 a6.4 a6.5 rvms-2* plants have no mature seeds. The long silique is filled with mature seeds. Bars, 2 mm. **C)** Alexander staining of the anther from WT, *rvms-2*, *a6.2 a6.3 a6.4*, *a6.2 a6.3 a6.4 rvms-2*, *a6.3 a6.4 a6.5*, *a6.3 a6.4 a6.5 rvms-2*, *a6-quad*, and *a6-quad rvms-2* mutants. Alexander staining analysis indicated no development of matured pollen in *rvms-2*, *a6.2 a6.3 a6.4 rvms-2*, and *a6.3 a6.4 a6.5 rvms-2* anthers under normal growth conditions. The anther was full with matured pollen grain in WT, *a6.2 a6.3 a6.4*, *a6.3 a6.4 a6.5*, *a6-quad*, and *a6-quad rvms-2* mutant under the same growth conditions. The matured pollen is purple, and the aborted pollen shows green. Images were digitally extracted for comparison. Bars, 50 μm. **D)** The rate of microspore release from the tetrads in *rvms-2* and *a6-quad rvms-2* anthers. The percentage was defined as the number of buds with tetrads divided by the total number of buds. Means with error bars indicate SD ( $n = 20$ ). A two-tailed t test was used to evaluate statistical significance difference (\*\* $P < 0.01$ ; ns,  $P > 0.05$ ; Supplementary Data Set 2).

mutants (Zhu et al. 2020; Wang et al. 2022). The reversible male sterile 2 (*rvms-2*) mutant exhibits severe male sterility under standard conditions, but low-temperature treatment can restore pollen development and plant fertility (Zhu et al. 2020). Subsequent studies suggest that low temperature defers A6 secretion from the tapetum into the locule which leads to delayed callose degradation and restoration of pollen development in *rvms-2* (Wang et al. 2022). To further verify the effects of a delay in callose degradation on pollen development, the *a6-quint* line was crossed with *rvms-2*. Due to the close linkage between A6 and RVMS-2, we only obtained *a6-quad rvms-2* (*a6.2 a6.3 a6.4 a6.5 rvms-2*) quintuple mutant. The *a6-quad rvms-2* lines ( $n > 20$ ) displayed increased fertility under normal conditions compared to *rvms-2*, whereas the *a6.2 a6.3 a6.4 rvms-2* and *a6.3 a6.4 a6.5 rvms-2* plants remained sterile (Fig. 4, A and B). It was further confirmed by Alexander's staining analysis. A substantial number of mature pollen grains were observed in *a6-quad rvms-2* while the complete abortion of pollen grains occurred in *rvms-2*, *a6.2 a6.3 a6.4 rvms-2* and *a6.3 a6.4 a6.5 rvms-2* plants (Fig. 4C). In the meantime, tetrad callose staining analysis showed a significant delay in tetrad callose degradation in *a6-quad rvms-2* compared to the *rvms-2* mutant (Fig. 4D). These findings demonstrated that loss of A6 function results in

delayed callose degradation, which can provide additional protection for pollen development in the anther.

### MYB80 and TEK coregulate A6 expression in the tapetum

Our previous studies demonstrated that the A6 is secreted into the locule rapidly after its synthesis in tapetum (Wang et al. 2022). To gain further insight into the gene expression pattern of A6s in anther, RNA in situ hybridization was used to reveal the expression pattern of A6, A6.2, and A6.3. Consistent with previous observations of A6-GFP (Wang et al. 2022) and tapetum transcriptomic data (Li et al. 2017a), A6 mRNA was specifically detected in the tapetum during Stage 7. A6.2 and A6.3 were also expressed in the tapetum but at a later period than A6 (Fig. 5A), suggesting that the tapetum-specific expression of A6s may have varied temporal patterns. As shown earlier, A6s were downregulated in *myb80 tek* (Fig. 2), so the dual-luciferase transient expression assay was used to investigate the involvement of MYB80 and TEK in regulating A6 expression. The results showed that MYB80 expression driven by the 35S promoter significantly induced the promoter activity of all 5 A6s ( $FC > 1.5$  and  $P < 0.05$ ) in *Arabidopsis* mesophyll protoplasts in comparison with the control groups (Fig. 5B). TEK expression driven by the 35S promoter activated 4 A6s: A6.2,

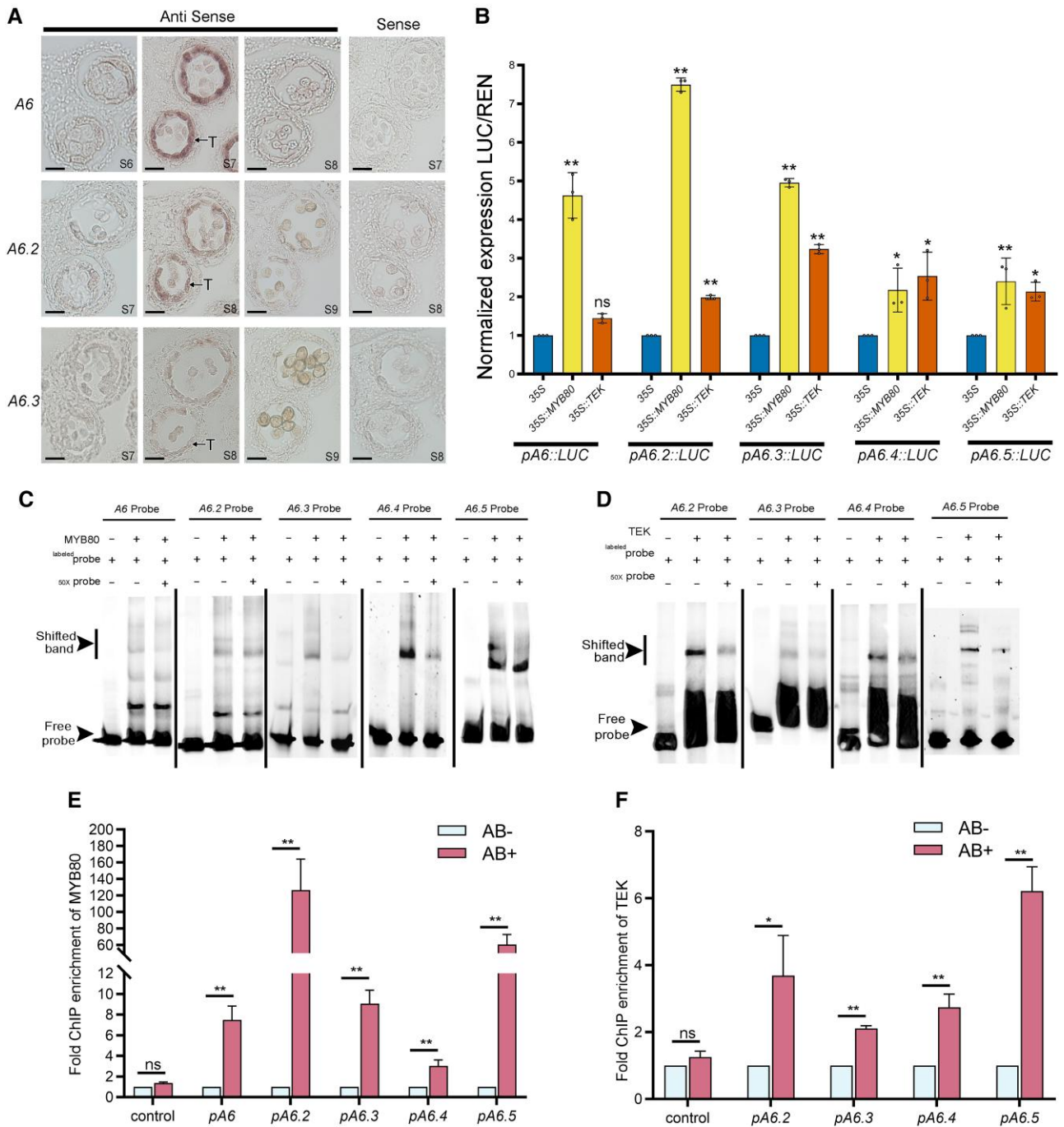


**Figure 5.** MYB80 and TEK directly regulate the expression of A6 members in tapetum. **A)** RNA in situ hybridization using antisense probe and sense probe to detect A6, A6.2, and A6.3 expression at anther Stages 6 to 9. T, tapetum. Bars, 20  $\mu$ m. **B)** Transient dual-luciferase transactivation of the MYB80 and TEK activate A6 expression in *Arabidopsis* leaf protoplasts. The reporters (*proA6.1::LUC*, *proA6.2::LUC*, *proA6.3::LUC*, *proA6.4::LUC*, and *proA6.5::LUC*) with effectors (*p35S::MYB80* and *p35S::TEK*) were transformed into protoplasts, respectively. The *p35S::REN* was used as an internal control, with the luciferase/renilla (LUC/REN) ratio set to 1. The significant activation of LUC/REN is  $\geq 2$  fold. Means with error bars indicate SD ( $n = 3$ ). A two-tailed t test was used to evaluate the statistical significance difference (LUC/REN  $\geq 2$  and  $*P < 0.05$ ,  $**P < 0.01$ ; ns, not significant (LUC/REN  $< 2$ ,  $P > 0.05$ ). **C to D)** Results from the EMSA show that MYB80 and TEK can bind to the fragment containing the predicted binding site in the A6 promoter region. Nonlabeled competitors are able to reduce the visible shift (arrow). **E to F)** ChIP-qPCR analysis of MYB80 and TEK enrichment on the A6 promoter. The inflorescence samples were obtained from MYB80-Myc and TEK-Flag transgenic plants. The DNA was recovered after the addition of the Myc or Flag antibody (AB+); the no-antibody (AB-) condition was used as the template. The enrichment of the A6 promoter fragments was confirmed by qPCR using the primers containing MYB80 and TEK binding sites, and primers without their binding sites were designed as control (as shown in [Supplementary Fig. S9](#)). The relative enrichment is presented compared with that of the AB- trial of each primer set. The means are shown with SD ( $n = 2$ ). ANOVA was used to evaluate the statistical significance difference between the binding set and the control set ( $**P < 0.01$ ;  $*P < 0.05$ ; ns,  $P > 0.05$ ; [Supplementary Data Set 2](#)).

A6.3, A6.4, and A6.5 (Figure 5B). These results confirm that MYB80 and TEK are able to respectively activate the expression of these A6s. MYB80 demonstrates a high binding affinity for the AACCA core (Phan et al. 2011; Xiong et al. 2016), while TEK is capable of

binding to AT-rich chromatin regions, including TTWTTTTTTT (T-box) and WADAWAYAWW sequences (van Drunen et al. 1997; Jia et al. 2015). These putative MYB80 and TEK binding sites were found in the promoters of these A6s (Supplementary Fig. S9).

Electrophoretic mobility shift assays (EMSA) and chromatin immunoprecipitation (ChIP) analyses were employed to determine the binding. The results from EMSA confirmed the ability of MYB80 to bind with the putative sites in the A6 promoters (Fig. 5C). Similarly, TEK also bound to the putative binding elements from the promoters of A6.2, A6.3, A6.4, and A6.5 (Figure 5D). Then, ChIP analysis was done using the transgenic lines of MYB80-Myc and TEK-Flag generated previously (Jia et al. 2015; Xiong et al. 2016). Quantitative ChIP-PCR (ChIP-qPCR) was performed using primers designed to promoter regions containing MYB80-binding or TEK-binding sites of the 5 A6 genes. Enrichment of the binding sites was detected in flower bud samples with AB+ (antibodies) compared to AB− (no antibodies), indicating that the MYB80-Myc and TEK-Flag proteins were positively enriched in these A6s' binding sites (ANOVA,  $P < 0.05$ ). Meanwhile, the enrichment was not detected in the control region (without MYB80 or TEK binding motifs) (Fig. 5, E and F). Taken together, these results demonstrate that MYB80 and TEK can directly regulate the expression of different A6s in the tapetum.

### Advanced expression of A6 and A6.2 leads to premature callose wall dissolution and abnormal exine formation

The timing of tetrad callose wall degradation associated with the pollen exine formation (Ariizumi and Toriyama 2011). Delayed callose degradation leads to abnormal exine development and reduces pollen viability under UV condition (Figs. 3 and 4). To further understand the importance of temporal control, we constructed advanced expression constructs of A6 and A6.2 driven by A9 promoter and transformed *Arabidopsis*. A9 is specifically expressed in the tapetum at Stages 5 to 9 (Feng and Dickinson 2010; Xu et al. 2015), which is earlier than MYB80, TEK (Zhang et al. 2007; Lou et al. 2014), and A6 (Fig. 5). The transgenic plants expressing A6 and A6.2 regulated by A9 promoter can be used to assess the effects of premature callose degradation on pollen development. The transgenic *promoterA9::A6* (WT) [*pA9::A6* (WT)] plants exhibited full fertility similar to WT plants, but the transgenic plants expressing *promoterA9::A6.2* (WT) [*pA9::A6.2* (WT)] plants were sterile (Supplementary Fig. S10), and no mature pollen grains could be observed in their anthers (Fig. 6A). SEM image showed a complete lack of sexine on *pA9::A6.2* (WT) pollen surface, whereas the sexine pattern of *pA9::A6* (WT) is basically normal (Fig. 6B). TEM was further used to exam the exine development in these lines. At Stage 7, the tetrads in the WT anther were formed with a thick layer of callose. In contrast, a thinner callose was observed in the transgenic *pA9::A6* (WT) (Fig. 6C), while the transgenic *pA9::A6.2* (WT) lines exhibited a more drastic reduction in callose, indicating a distinct callose degradation ability of A6 and A6.2. By the end of Stage 9, exine development was almost complete in both WT and *pA9::A6* (WT) transgenic plants. However, the sexine structure was absent in the *pA9::A6.2* (WT) microspores, with poorly formed tectum and columella skeletons (Fig. 6C). Taken together, these findings demonstrate that strict regulation of callose degradation under the control of MYB80 and TEK is essential for exine patterning and male fertility.

## Discussion

### A6s are involved in tetrad callose wall degradation

The primary constituent of the callose wall in the tetrad is  $\beta$ -1,3-glucan. Previous biochemical investigations have demonstrated

that enzymes similar to the *Arabidopsis* A6 possess the ability to break down  $\beta$ -1,3-glucan and potentially play a role in degrading the callose of tetrad wall (Stieglitz and Stern 1973; Stieglitz 1977; Worrall et al. 1992). However, a single mutation of A6 does not exhibit a significant phenotypic defect in callose degradation (Wang et al. 2022; Fig. 2), which is caused by the functional redundancy of other A6 family members as shown in this study. In the quintuple mutant of A6s, *a6-quint*, the degradation process of tetrad wall was significantly delayed and affected pollen wall formation (Figs. 2 and 3). In garlic (*Allium sativum*), distinct peaks of callase activity at 3 specific pH values suggest the existence of 3 isoforms, each active under different pH conditions (Winiarczyk et al. 2012). Phylogenetic analysis shows these 5 A6 members are grouped into 3 distinct subfamilies (Supplementary Fig. S3). These indicate that the 5 A6 members form 3 functional types of callase. This diversity may facilitate both rapid callose wall degradation and necessary for pollen wall formation under different conditions. In *a6-quint* anthers, the callose degradation eventually completed at the later stages of anther development, and microspores were released (Fig. 2), indicating the role of other A6s aside from the main 5 A6s as 17 A6 homologs were identified in the tapetum (Supplementary Figs. S3 and S4). This also explains the difficulty in identifying *a6* mutants with incomplete callose degradation. In petunia (*Petunia hybrida*) and lily (*Lilium*) anthers, callase activity follows a tightly regulated developmental pattern. It is initially low during the early meiotic stage but increases sharply, peaking at microspore release (Frankel et al. 1969; Steiglitz and Stern 1973; Steiglitz 1977). The in situ hybridization data indicate varied temporal expression patterns of A6, A6.2, and A6.3 within the tapetum (Fig. 5). Protein structure analysis reveals minimal differences between A6 and A6.2 (Supplementary Figure S3). However, the premature expression of A6.2 led to earlier callose degradation of tetrad wall and loss of exine whereas the premature expression of A6 has a minimal effect on the callose wall and exine development (Fig. 6). These suggest that A6 family members may have distinct enzyme activities with different activators or inhibitors, and with well-coordinated temporal and spatial expression patterns, to participate in the pollen wall remodeling from tetrads to microspores.

### Tetrad wall degradation and pollen wall formation are both regulated by the AMS-MYB80/TEK pathway

The tetrad wall consists mainly of pectin and callose. MYB80 directly controls the pectin degradation that involves QUARTET (QRTs) (Preuss et al. 1994; Shi et al. 2021). This study demonstrated the involvement of A6 family in callose degradation at the tetrad stage during the anther development (Fig. 2), and the expression of 5 A6s was shown to be directly regulated by MYB80 while TEK also regulates A6.2 to A6.5 (Figures 2 and 5). Therefore, these findings suggest the important role of MYB80 in the degradation of both structural components of the tetrad wall, but the function of TEK is limited to regulate the callose degradation. Following the degradation of tetrad wall, microspores are released and subsequently develop into mature pollen that is encapsulated by an outer exine layer and an inner intine layer (Scott et al. 2004). The exine includes sexine and nexine layers. The mutation of MYB80 results in the complete loss of the sexine (Zhang et al. 2007), which is consistent with its role in regulating the expression of several sporopollenin synthesis genes that are crucial for the formation of sexine (Wang et al. 2018). The mutation of TEK does not affect sexine development but causes the complete absence of nexine which leads to the rupture of pollen after the pollen is released. Both TEK and MYB80 are

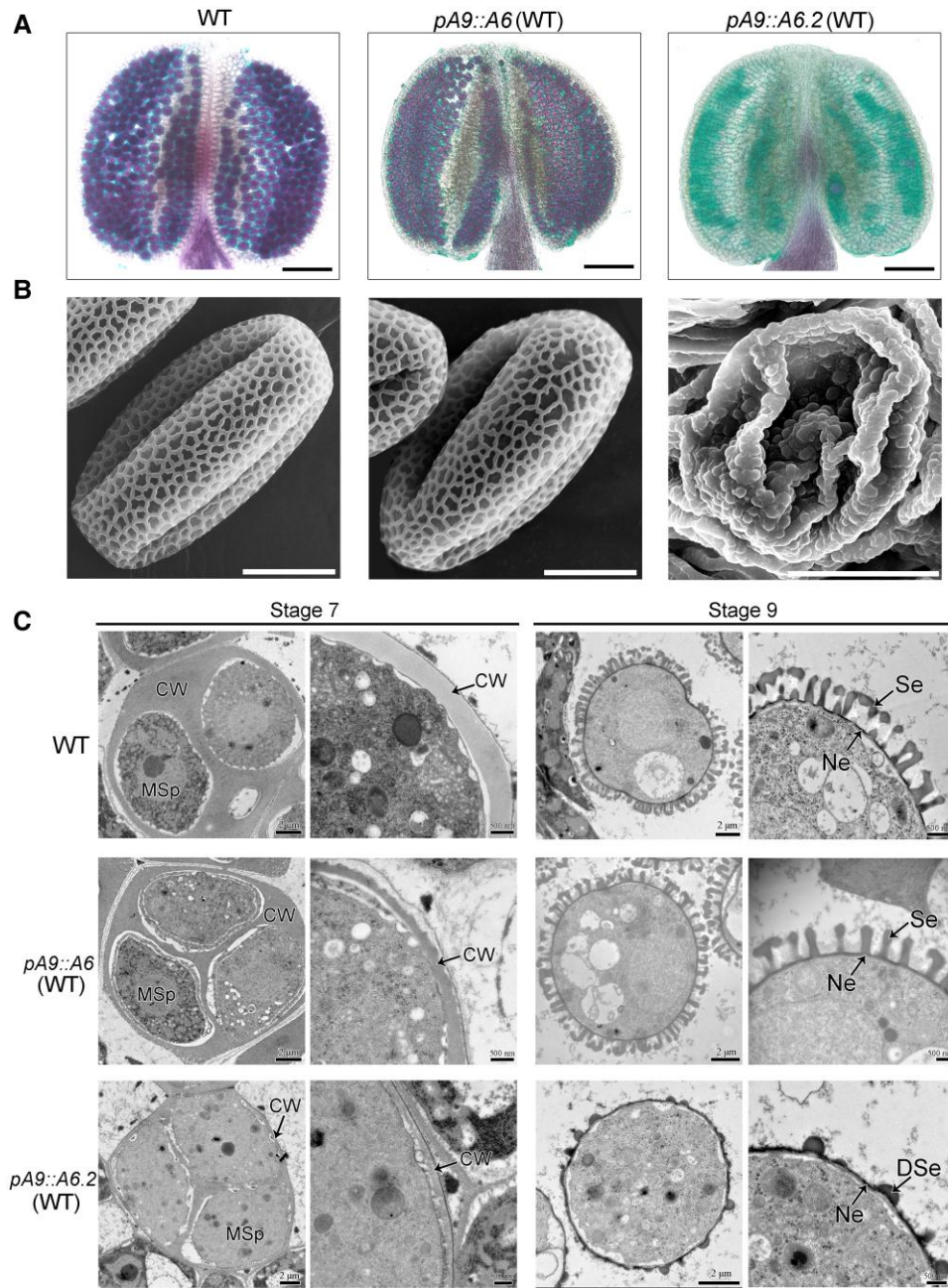


**Figure 6.** Advanced expression of A6 and A6.2 leads to premature tetrad callose wall degradation and impairs sexine formation. **A)** Alexander staining of the anthers from wild-type (WT), pA9::A6 (WT), and pA9::A6.2 (WT) plants. Bars, 1 mm. The matured pollen is purple, and the aborted pollen is green. Images were digitally extracted for comparison. The WT image was reused from [Supplementary Figure S2B](#). **B)** Scanning electron micrograph of the pollen grains from WT, pA9::A6 (WT), and pA9::A6.2 (WT) plants. Bars, 10  $\mu$ m. The latticed exine is absent from aborted pollen in pA9::A6.2 (WT) anthers. **C)** TEM images of callose wall and pollen wall in WT, pA9::A6 (WT), and pA9::A6.2 (WT) transgenic plants at Stages 7 and 9. The thickness of the tetrad callose wall was decreased in pA9::A6 (WT) and pA9::A6.2 (WT) anthers when microspores membrane undulations emerged within the callose wall at early Stage 7. At Stage 9, pA9::A6.2 (WT) pollens have a normal nexine layer with a defective sexine structure. The right image of pA9::A6.2 (WT) at Stage 7 is an enlargement of its left image. CW, callose wall; Ne, nexine; Se, sexine; Msp, microspore; DSe, defective sexine.

directly regulated by AMS ([Lou et al. 2014](#)). Our results indicate that the double mutation of *myb80 tek*, similar to *ams*, results in the complete loss of the pollen exine structure ([Supplementary Fig. S1](#)). Therefore, the AMS-MYB80/TEK pathway directly regulates both the degradation of the tetrad wall and the formation of exine layer ([Fig. 7](#)). While the defective exine leads to pollen abortion, the delayed degradation of callose can offer additional protection ([Wang et al. 2022](#)), allowing these mutants to form functional pollen ([Fig. 4](#)). Plant cells are generally protected by the cell wall. Tetrads

and pollen are shielded by the tetrad wall and the pollen wall, respectively ([Scott et al. 2004](#); [Ariizumi and Toriyama 2011](#); [Shi et al. 2015](#); [Radja et al. 2019](#)). The timing of callose wall degradation is critical. Both delayed or premature degradation can disrupt the normal structure of exine and affect pollen fertility ([Figs. 3 and 6](#)). Hence, the AMS-MYB80/TEK pathway plays an essential role in male reproductive development in plants through its direct regulation of cell wall transition and remodeling of tetrad and microspores.

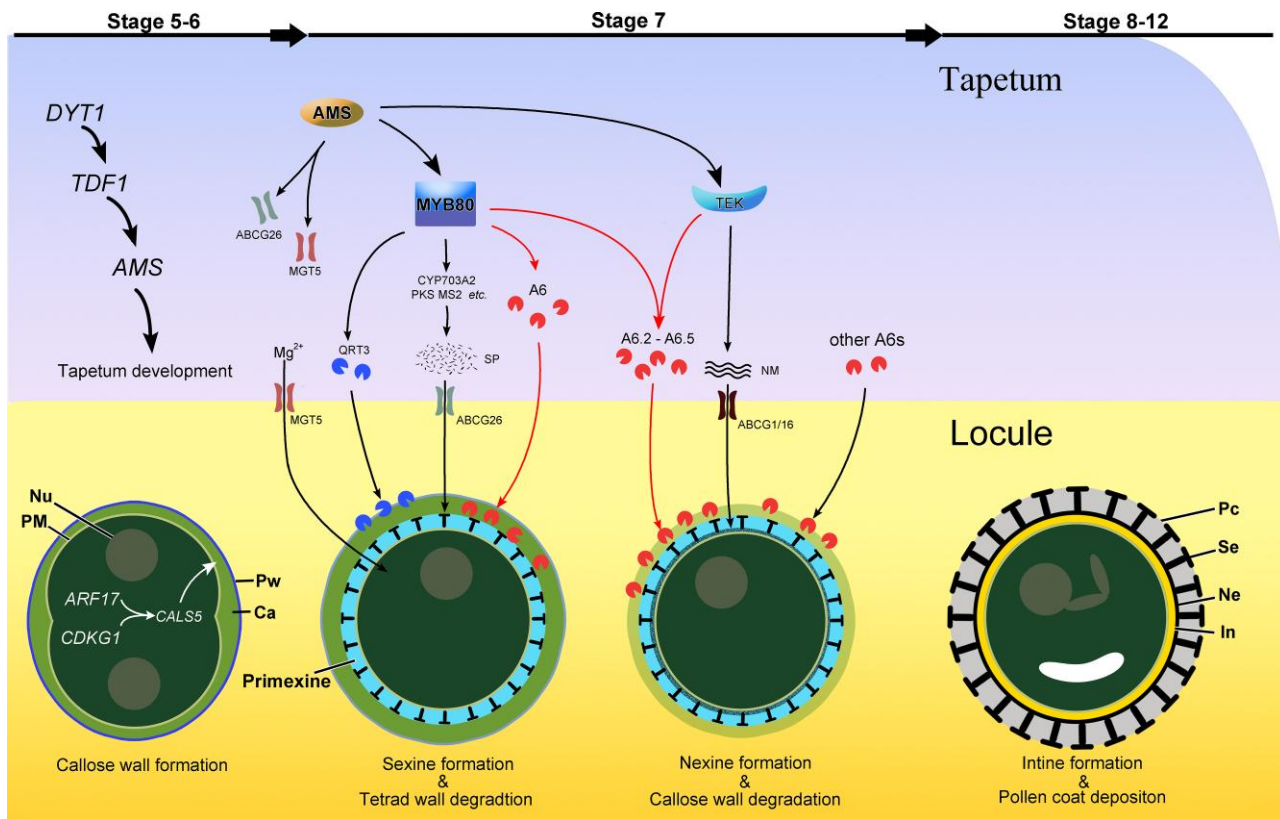


**Figure 7.** Schematic diagram of the genetic pathway controlling tetrad wall and pollen development in *Arabidopsis*. During Stages 5 to 6 of anther development, the tapetal cells differentiate and develop under the regulation of the DTY1-TDF1-AMS pathway (Zhu et al. 2011). In microspore mother cells, AUXIN RESPONSE FACTOR 17 (ARF17) and CYCLIN-DEPENDENT KINASE G1 (CDKG1) regulate CALLOSE SYNTHASE 5 (Cals5) expression to facilitate tetrad callose wall deposition (Huang et al. 2013; Yang et al. 2013). AMS directly regulates ATP-binding cassette G26 (ABCG26) and MAGNESIUM TRANSPORT 5 (MGT5) to participate in sporopollenin and magnesium transport (Xu et al. 2014; Xu et al. 2015). TEK and MYB80 regulated by AMS are responsible for the formation of nexine and sexine, respectively (Lou et al. 2014). MYB80 directly regulates QUARTET 3 (QRT3) for Pw degradation (Shi et al. 2021). Meanwhile, MYB80 initiates sporopollenin synthesis for sexine development. With the formation of the “T” shaped prosexine within primexine, MYB80 also directly regulates the expression of A6 in the tapetum, which is subsequently secreted into the anther locule to degrade callose wall while the nexine materials gradually accumulate between the microspore plasma membrane and sexine under the control of TEK. The rapid degradation of the callose wall results from the expression of 5 A6s under direct regulation of MYB80 and TEK in the tapetum. There are other unidentified A6 proteins in the tapetum that act as a final safeguard for callose wall degradation. After microspore releases from the tetrad, the intine layer and fine sexine layer filled with pollen coat are formed. Nu, nucleus; Ca, callose; PM, plasma membrane; Pw, primary cell wall; Sp, sporopollenin; NM, nexin materials; Pc, pollen coat; In, intine; Ne, nexin; Se, sexine.

## Materials and methods

### Plant materials and growth conditions

The *Arabidopsis* (*Arabidopsis thaliana*) wild-type (WT) and mutants are in the Columbia-0 (Col-0) background. Plants were grown under normal conditions (16 h of light at 22°C/8 h of darkness at 18°C with approximately 60% to 80% relative humidity). The potting mix consisted of mainly vermiculite and 0.1% chemical fertilizer (Shanghai Wintong Chemicals Co., Ltd.). *ams*, *tek*, *myb80*, and *rvms-2* mutants are from our laboratory seed stock. *a6* (AT4G14080), *a6.2* (AT3G23770), *a6.3* (AT4G26830), *a6.4* (AT3G46570), and *a6.5* (AT5G64790) T-DNA insertion mutant lines were obtained from the *Arabidopsis* Biological Resource Center (ABRC) (<https://abrc.osu.edu>). The T-DNA insertion site for each line was shown (Supplementary Fig. S5). *myb80 tek*, double mutant (*a6 a6.2*), triple mutant (*a6 a6.2 a6.3*), quadruple mutant (*a6.2 a6.3 a6.4 a6.5*, *a6-quad*), quintuple mutant (*a6 a6.2 a6.3 a6.4 a6.5*, *a6-quint*), *a6.2 a6.3 a6.4 rvms-2*, *a6.3 a6.4 a6.5 rvms-2*, and *a6-quad rvms-2* were generated by crossing. The primers used for genotyping are listed in Supplementary Data Set 1. The plants were imaged with a Nikon digital camera (Nikon, Japan).

### Microscopy

Alexander staining solution was made by mixing 10 ml ethanol, 1 ml of 1% malachite green in 95% ethanol, 50 ml distilled H<sub>2</sub>O, 25 ml glycerol, 5 g phenol, 5 g chloral hydrate, 5 ml of 1% acid fuchsin in H<sub>2</sub>O, 0.5 ml of 1% orange G in H<sub>2</sub>O, and 1 ml 4% glacial acetic acid. After staining, the anthers were incubated at room temperature overnight, and then the stain was washed away and observed under a microscope. For semithin section, the flower buds embedded in Spurr's resin were cross-sectioned with a glass knife to obtain semithin section at a thickness of 1 μm. Some sections were incubated in 0.01% toluidine blue for 5 min at 45°C, washed with H<sub>2</sub>O, and observed under bright-field microscopy, and some were stained in 0.1% aniline blue staining solution for 5 min for observation of callose under a fluorescence microscope with UV light. For SEM, the pollen grains were coated with gold-palladium (8 nm) and examined under a JSM-840 microscope (JEOL, Japan). For TEM, the flower buds were fixed with 2.5% (v/v) glutaraldehyde in 0.1 M phosphate buffer (pH 7.2), washed several times, postfixed in osmium tetroxide overnight, gradient dehydrated, and embedded in Spurr's resin. The ultrathin sections were examined under a transmission electron microscopy (Hitachi H-7650, Japan).

## Statistical analysis of tetrad callose staining

The plant materials used in this experiment were grown under similar conditions. The main inflorescences showing vigorous and similar growth were selected and were fixed in chloroform-acetic acid-alcohol fixative solution. In order to statistically analyze the callose degradation process, the flower buds were observed, and their sizes were measured based on the photos taken from a DX51 digital camera (Olympus, Japan). The buds were then dissected and the anthers were stained with aniline blue solution. The differences in tetrad development in the buds of each group were statistically analyzed ([Supplementary Data Set 2](#)) as described previously ([Wang et al. 2022](#)).

## Plasmid construction and identification of transgenic plants

The plasmids, *proA9::A6* and *proA9::A6.2*, were generated by ligating the promoter of A9 (1,865 bp) with the genomic sequence of A6 (1,596 bp) and A6.2 (1,641 bp) respectively. Similarly, *proTEK::A6* and *proTEK::A6.2* constructs were generated using the TEK promoter (725 bp) and A6, A6.2 genomic sequence. All the above promoter and gene sequences were amplified using KOD polymerase (Takara, Japan, [www.takara.com](http://www.takara.com)), and proper restriction enzyme sites (BamHI and/or EcoRI) were added at each end by PCR. The recombinant vectors (pCAMBIA1300 binary vector, CAMBIA, Australia) were constructed by homologous recombination. These vectors were transferred into *Agrobacterium tumefaciens* GV3101 which was used for plant transformation using the floral dipping method. The transgenic plants were identified on Murashige and Skoog medium containing hygromycin. At least 3 independent and phenotypically similar lines were obtained for each transgenic construct, and the T<sub>2</sub> generation of the most phenotypically stable line was selected for analysis. The T<sub>1</sub> generation of transgenic lines with sterile phenotypes was crossed with WT, and the T<sub>2</sub> generation was screened for plants that exhibited a phenotype identical to that of the parental plants for analysis. The sequences of all the primers used are provided in [Supplementary Data Set 1](#).

## In vitro pollen germination

The collected pollen grains were spread on the germination medium as described previously ([Xue et al. 2020](#)), and some of them were irradiated with ultraviolet light. Pollen was germinated at 24°C for 16 h and then observed under a light microscope (Olympus BX51 microscope equipped with a digital camera). More than 100 pollen grains were counted for each experimental repeat to calculate the germination rate. The successful germination was counted only when the pollen tubes were longer than the diameter of the pollen grain. Mean germination rate and standard deviation (SD) were calculated from 3 biological repeats ([Supplementary Data Set 2](#)).

## RT-qPCR assay

Total RNA was extracted from the inflorescences of WT and mutant plants using a TRIzol kit (Life Technologies, United States). RT-qPCR was performed using SYBR Green Real-Time PCR Master Mix (Toyobo, Japan) on ABI 7300 (Applied Biosystems, United States). Relative expression levels were normalized with *TUBULIN BETA8* (*TUB*) served as an internal standard. The data are presented as the means with the SD of 3 biological replicates and the primers used are listed in [Supplementary Data Set 1](#).

## RNA in situ hybridization

RNA in situ hybridization was performed as described previously ([Xu et al. 2015](#)). Flower samples were fixed in FAA solution, dehydrated using ethanol gradient, embedded in wax, and sectioned with a rotary microtome (MR2; RMC, United States). Digoxigenin (DIG)-labeled A6 probes were synthesized by PCR using DIG RNA Labeling Kit (Roche, United States). A6 cDNA fragment (100 to 150 bp) was amplified by A6-specific primers that added restriction enzyme sites (BamHI and EcoRI). PCR products were cloned into the pbluescriptSK vector and confirmed by sequencing. The resultant plasmids were linearized and used as the template for transcription with T3 or T7 RNA polymerase, respectively. The primers used are listed in [Supplementary Data Set 1](#).

## Electrophoretic mobility shift assays

To obtain purified TEK and MYB80 proteins ([Jia et al. 2015](#); [Xiong et al. 2016](#)) for EMSA experiments, primers were designed to amplify the full-length fragments of TEK and MYB80 genes. Then the full-length CDS of TEK was cloned into the Pet-51b vector to generate the HIS-TEK construct, and MYB80 CDS was cloned into the pMAL-p5X vector to generate the MBP-MYB80 construct. The fusion proteins were produced and purified according to the manufacturer's instructions (Thermo Fisher Scientific, Inc.). The DNA fragments containing the TEK regulatory region (AT-rich sequence) and the MS188 regulatory region (AACCA) through specific primers were synthesized to generate biotin-labeled probes and competitive probes, respectively. EMSA was performed with a Lightshift Chemiluminescent EMSA kit (Thermo Scientific, United States) according to the manufacturer's instructions. The images were obtained with a Tanon-5500 Chemiluminescent Imaging System (Tanon, China).

## Chromatin immunoprecipitation

Inflorescences of AMS-MYC and TEK-Flag transgenic lines ([Lou et al. 2014](#); [Xu et al. 2015](#)) were used for Chromatin immunoprecipitation using the protocol prescribed previously ([Lou et al. 2014](#)). Briefly, flower bud tissue (1 g) was crosslinked with formaldehyde. Chromatin was sonicated to obtain fragments with an average size ranging between 200 and 800 bp. Antibody-protein-DNA complexes were precipitated with protein G magnetic beads (Invitrogen, United States). After purification, DNA fragments were used for qPCR analysis. [Supplementary Data Set 1](#) lists the primer sequences used for ChIP.

## Dual-luciferase transient expression assays in *Arabidopsis* protoplasts

For the dual-luciferase transient expression assays, the ~2 kb promoters of A6s were cloned and constructed into the pGreen II 0800-luc vector. To generate effector constructs, the full-length coding sequences of MYB80 and TEK were inserted into the pCAMBIA1300 binary vector to generate 35S::MYB80 and 35S::TEK fusion vectors, and the pCAMBIA1300 empty vector was used as a control. A restriction enzyme site (BamHI) was added at each end of those fragments for recombinant vector construction. The *Arabidopsis* protoplasts were used for this assay. The luciferase assays were performed as previously described ([Qiu et al. 2015](#)). [Supplementary Data Set 1](#) lists the primer sequences used for clone promoters of A6s.

## Phylogenetic analyses of A6 proteins in *Arabidopsis*

The amino acid sequences for A6 proteins of *Arabidopsis* were downloaded from TAIR ([www.arabidopsis.org](http://www.arabidopsis.org)). A phylogenetic tree of A6 members in *Arabidopsis* was constructed with MEGA-X by the neighbor-joining (NJ) method and 1,000 bootstrap replicates and selection of Bootstrap trees. The 3D structures of A6 and A6.2 were predicted using the AlphaFold 3 protein structure database.

## Statistical analysis

The significance of differences for pairwise comparisons was estimated by means of a two-tailed Student's *t* test in Microsoft Excel 2020, with the following levels of significance: \**P* < 0.05 and \*\**P* < 0.01. One-way and two-way ANOVA analyses were conducted using GraphPad Prism 9.0, followed by the least significant difference test at \**P* < 0.05 and \*\**P* < 0.01. The statistical data are provided in [Supplementary Data Set 2](#).

## Accession numbers

Sequence data from this article can be found in the GenBank/EMBL data libraries under accession numbers A6 (AT4G14080), A6.2 (AT3G23770), A6.3 (AT4G26830), A6.4 (AT3G46570), A6.5 (AT5G64790), A6.6 (AT5G55180), A6.7 (AT3G07320), A6.8 (AT2G05790), A6.9 (AT5G56590), A6.10 (AT4G34480), A6.11 (AT2G01630), A6.12 (AT3G55430), A6.13 (AT5G42100), A6.14 (AT3G24330), A6.15 (AT4G17180), A6.16 (AT5G58090), A6.17 (AT5G20870), AMS (AT2G16910), MYB80 (AT5G56110), TEK (AT2G42940), RVMS-2 (AT4G10950), and TUB (AT5G23860).

## Acknowledgments

We appreciate Prof. Zaibao Zhang, Prof. Shui Wang, and Prof. Qingbo Yu for critical discussions and Dr. Yanshuang Liu for providing analytical assistance.

## Author contributions

X.X. and Z.-N.Y. conceived and supervised the project; X.X., K.W., and Y.Y. performed most of the experiments; N.Y. performed the TEM experiment; X.Z., X.Q., and Y.G. performed the dual-luciferase transient expression, ChIP assays, and EMSAs; X.X., K.W., Y.L., P.X., and Z.-N.Y. wrote the manuscript. All authors read and approved the final manuscript.

## Supplementary data

The following materials are available in the online version of this article.

**Supplementary Figure S1.** Exine is completely absent in *myb80 tek* anthers.

**Supplementary Figure S2.** Phenotype of single and multiple T-DNA insertion mutant of five A6 genes.

**Supplementary Figure S3.** Homology and phylogenetic analysis of A6 in *Arabidopsis*.

**Supplementary Figure S4.** Expression of 48 homologous genes of A6 in tapetum.

**Supplementary Figure S5.** RT-qPCR analysis of the expression level of 17 tapetal expressed A6 genes in *ams* inflorescences.

**Supplementary Figure S6.** *pTEK::A6* and *pTEK::A6.2* can complement callose degradation in *myb80 tek* mutant.

**Supplementary Figure S7.** Callose deposition was not affected in *a6-quint* mutant.

**Supplementary Figure S8.** Phenotype of sexine pattern in *a6-quint* and multiple mutants of five A6s.

**Supplementary Figure S9.** Schematic diagram of MYB80 and TEK binding sites in A6 promoter.

**Supplementary Figure S10.** Phenotype of WT plants transgenic with *pA9::A6* and *pA9::A6.2* constructions.

**Supplementary Data Set 1.** Primers used in this study.

**Supplementary Data Set 2.** Summary of statistical analyses.

## Funding

This work was supported by the National Natural Science Foundation of China (Grant numbers 32470345 and 31900260) and Shanghai Engineering Research Center of Plant Germplasm Resources (Grant number 17DZ2252700).

**Conflict of interest statement.** The authors have declared that no conflict of interest exists.

## Data availability

The data underlying this article are available in the article and in its online supplementary material.

## References

- Ariizumi T, Toriyama K. Genetic regulation of sporopollenin synthesis and pollen exine development. *Annu Rev Plant Biol.* 2011;62(1):437–460. <https://doi.org/10.1146/annurev-arplant-042809-112312>
- Blackmore S, Wortley AH, Skvarla JJ, Rowley JR. Pollen wall development in flowering plants. *New Phytol.* 2007;174(3):483–498. <https://doi.org/10.1111/j.1469-8137.2007.02060.x>
- Dong X, Hong Z, Sivaramakrishnan M, Mahfouz M, Verma DP. Callose synthase (CalS5) is required for exine formation during microgametogenesis and for pollen viability in *Arabidopsis*. *Plant J.* 2005;42:315–328. <https://doi.org/10.1111/j.1365-313X.2005.02379.x>
- Enns LC, Kanaoka MM, Torii KU, Comai L, Okada K, Cleland RE. Two callose synthases, GSL1 and GSL5, play an essential and redundant role in plant and pollen development and in fertility. *Plant Mol Biol.* 2005;58(3):333–349. <https://doi.org/10.1007/s11103-005-4526-7>
- Feng X, Dickinson HG. Tapetal cell fate, lineage and proliferation in the *Arabidopsis* anther. *Development.* 2010;137(14):2409–2416. <https://doi.org/10.1242/dev.049320>
- Frankel R, Izhar S, Nitsan J. Timing of callase activity and cytoplasmic male sterility in *Petunia*. *Biochem Genet.* 1969;3(5):451–455. <https://doi.org/10.1007/BF00485605>
- Heslop-Harrison J. Pollen wall development. The succession of events in the growth of intricately patterned pollen walls is described and discussed. *Science.* 1968;161(3838):230–237. <https://doi.org/10.1126/science.161.3838.230>
- Hird DL, Worrall D, Hodge R, Smartt S, Paul W, Scott R. The anther-specific protein encoded by the *Brassica napus* and *Arabidopsis thaliana* A6 gene displays similarity to beta-1,3-glucanases. *Plant J.* 1993;4(6):1023–1033. <https://doi.org/10.1046/j.1365-313X.1993.04061023.x>
- Huang XY, Niu J, Sun MX, Zhu J, Gao JF, Yang J, Zhou Q, Yang ZN. CYCLIN-DEPENDENT KINASE G1 is associated with the spliceosome to regulate CALLOSE SYNTHASE5 splicing and pollen wall

- formation in *Arabidopsis*. *Plant Cell*. 2013;25(2):637–648. <https://doi.org/10.1105/tpc.112.107896>
- Izhar S, Frankel R. Mechanism of male sterility in *Petunia*: the relationship between pH, callase activity in the anthers, and the breakdown of the microsporogenesis. *Theor Appl Genet*. 1971;41(3):104–108. <https://doi.org/10.1007/BF00277751>
- Jia QS, Zhu J, Xu XF, Lou Y, Zhang ZL, Zhang ZP, Yang ZN. *Arabidopsis* AT-hook protein TEK positively regulates the expression of arabinogalactan proteins for Nexine formation. *Mol Plant*. 2015;8(2):251–260. <https://doi.org/10.1016/j.molp.2014.10.001>
- Li DD, Xue JS, Zhu J, Yang ZN. Gene regulatory network for tapetum development in *Arabidopsis thaliana*. *Front Plant Sci*. 2017;a:8:1559. <https://doi.org/10.3389/fpls.2017.01559>
- Li WL, Liu Y, Douglas CJ. Role of glycosyltransferases in pollen wall primexine formation and exine patterning. *Plant Physiol*. 2017b;173(1):167–182. <https://doi.org/10.1104/pp.16.00471>
- Liu XQ, Liu ZQ, Yu CY, Dong JG, Hu SW, Xu AX. TGMS in rapeseed (*Brassica napus*) resulted in aberrant transcriptional regulation, asynchronous microsporocyte meiosis, defective tapetum, and fused sexine. *Front Plant Sci*. 2017;8:1268. <https://doi.org/10.3389/fpls.2017.01268>
- Lou Y, Xu XF, Zhu J, Gu JN, Blackmore S, Yang ZN. The tapetal AHL family protein TEK determines nexine formation in the pollen wall. *Nat Commun*. 2014;5(1):3855. <https://doi.org/10.1038/ncomms4855>
- Lu P, Chai M, Yang J, Ning G, Wang G, Ma H. The *Arabidopsis* CALLOSE DEFECTIVE MICROSPORE1 gene is required for male fertility through regulating callose metabolism during microsporogenesis. *Plant Physiol*. 2014;164(4):1893–1904. <https://doi.org/10.1104/pp.113.233387>
- Nishikawa S, Zinkl GM, Swanson RJ, Maruyama D, Preuss D. Callose (beta-1,3 glucan) is essential for *Arabidopsis* pollen wall patterning, but not tube growth. *BMC Plant Biol*. 2005;5(1):22. <https://doi.org/10.1186/1471-2229-5-22>
- Phan HA, Iacuone S, Li SF, Parish RW. The MYB80 transcription factor is required for pollen development and the regulation of tapetal programmed cell death in *Arabidopsis thaliana*. *Plant Cell*. 2011;23(6):2209–2224. <https://doi.org/10.1105/tpc.110.082651>
- Preuss D, Rhee SY, Davis RW. Tetrad analysis possible in *Arabidopsis* with mutation of the QUARTET (QRT) genes. *Science*. 1994;264(5164):1458–1460. <https://doi.org/10.1126/science.8197459>
- Qiu K, Li Z, Yang Z, Chen J, Wu S, Zhu X, Gao S, Gao J, Ren G, Kuai B, et al. EIN3 and ORE1 accelerate degreening during ethylene-mediated leaf senescence by directly activating chlorophyll catabolic genes in *Arabidopsis*. *PLoS Genet*. 2015;11(7):e1005399. <https://doi.org/10.1371/journal.pgen.1005399>
- Radja A, Horsley EM, Lavrentovich MO, Sweeney AM. Pollen cell wall patterns form from modulated phases. *Cell*. 2019;176(4):856–868.e810. <https://doi.org/10.1016/j.cell.2019.01.014>
- Rozema J, Broekman RA, Blokker P, Meijkamp BB, de Bakker N, van de Staaij J, van Beem A, Ariese F, Kars SM. UV-B absorbance and UV-B absorbing compounds (para-coumaric acid) in pollen and sporopollenin: the perspective to track historic UV-B levels. *J Photochem Photobiol B*. 2001;62(1–2):108–117. [https://doi.org/10.1016/S1011-1344\(01\)00155-5](https://doi.org/10.1016/S1011-1344(01)00155-5)
- Sanders P, Bui A, Weterings K, McIntire K, Hsu Y-C, Lee P, Truong M, Beals T, Goldberg R. Anther developmental defects in *Arabidopsis thaliana* male-sterile mutants. *Sex Plant Reprod*. 1999;11(6):297–322. <https://doi.org/10.1007/s004970050158>
- Scott RJ, Spielman M, Dickinson HG. Stamen structure and function. *Plant Cell*. 2004;16(suppl\_1):S46–S60. <https://doi.org/10.1105/tpc.017012>
- Shi J, Cui M, Yang L, Kim YJ, Zhang D. Genetic and biochemical mechanisms of pollen wall development. *Trends Plant Sci*. 2015;20(11):741–753. <https://doi.org/10.1016/j.tplants.2015.07.010>
- Shi QS, Lou Y, Shen SY, Wang SH, Zhou L, Wang JJ, Liu XL, Xiong SX, Han Y, Zhou HS, et al. A cellular mechanism underlying the restoration of thermo/photoperiod-sensitive genic male sterility. *Mol Plant*. 2021;14(12):2104–2114. <https://doi.org/10.1016/j.molp.2021.08.019>
- Stieglitz H. Role of beta-1,3-glucanase in postmeiotic microspore release. *Dev Biol*. 1977;57(1):87–97. [https://doi.org/10.1016/0012-1606\(77\)90356-6](https://doi.org/10.1016/0012-1606(77)90356-6)
- Stieglitz H, Stern H. Regulation of beta-1,3-glucanase activity in developing anthers of *Lilium*. *Dev Biol*. 1973;34(1):169–173. [https://doi.org/10.1016/0012-1606\(73\)90347-3](https://doi.org/10.1016/0012-1606(73)90347-3)
- Tidy AC, Ferjentsikova I, Vizcay-Barrena G, Liu B, Yin W, Higgins JD, Xu J, Zhang D, Geelen D, Wilson ZA. Sporophytic control of pollen meiotic progression is mediated by tapetum expression of ABORTED MICROSPORES. *J Exp Bot*. 2022;73(16):5543–5558. <https://doi.org/10.1093/jxb/erac225>
- Toller A, Brownfield L, Neu C, Twell D, Schulze-Lefert P. Dual function of *Arabidopsis* glucan synthase-like genes GSL8 and GSL10 in male gametophyte development and plant growth. *Plant J*. 2008;54(5):911–923. <https://doi.org/10.1111/j.1365-3113X.2008.03462.x>
- van Drunen CM, Oosterling RW, Keultjes GM, Weisbeek PJ, van Driel R, Smeekens SC. Analysis of the chromatin domain organisation around the plastocyanin gene reveals an MAR-specific sequence element in *Arabidopsis thaliana*. *Nucleic Acids Res*. 1997;25(19):3904–3911. <https://doi.org/10.1093/nar/25.19.3904>
- Wan L, Zha W, Cheng X, Liu C, Lv L, Liu C, Wang Z, Du B, Chen R, Zhu L, et al. A rice beta-1,3-glucanase gene *Osg1* is required for callose degradation in pollen development. *Planta*. 2011;233(2):309–323. <https://doi.org/10.1007/s00425-010-1301-z>
- Wang K, Guo ZL, Zhou WT, Zhang C, Zhang ZY, Lou Y, Xiong SX, Yao XZ, Fan JJ, Zhu J, et al. The regulation of sporopollenin biosynthesis genes for rapid pollen wall formation. *Plant Physiol*. 2018;178(1):283–294. <https://doi.org/10.1104/pp.18.00219>
- Wang KQ, Yu YH, Jia XL, Zhou SD, Zhang F, Zhao X, Zhai MY, Gong Y, Lu JY, Guo Y, et al. Delayed callose degradation restores the fertility of multiple P/TGMS lines in *Arabidopsis*. *J Integr Plant Biol*. 2022;64(3):717–730. <https://doi.org/10.1111/jipb.13205>
- Winiarczyk K, Jaroszuk-Scisiel J, Kupisz K. Characterization of callase (beta-1,3-D-glucanase) activity during microsporogenesis in the sterile anthers of *Allium sativum* L. and the fertile anthers of *A. atropurpureum*. *Sex Plant Reprod*. 2012;25(2):123–131. <https://doi.org/10.1007/s00497-012-0184-5>
- Worrall D, Hird DL, Hodge R, Paul W, Draper J, Scott R. Premature dissolution of the microsporocyte callose wall causes male sterility in transgenic tobacco. *Plant Cell*. 1992;4(7):759–771. <https://doi.org/10.1105/tpc.4.7.759>
- Xiong SX, Lu JY, Lou Y, Teng XD, Gu JN, Zhang C, Shi QS, Yang ZN, Zhu J. The transcription factors MS188 and AMS form a complex to activate the expression of CYP703A2 for sporopollenin biosynthesis in *Arabidopsis thaliana*. *Plant J*. 2016;88(6):936–946. <https://doi.org/10.1111/tpj.13284>
- Xu J, Ding Z, Vizcay-Barrena G, Shi J, Liang W, Yuan Z, Werck-Reichhart D, Schreiber L, Wilson ZA, Zhang D. ABORTED MICROSPORES acts as a master regulator of pollen wall formation in *Arabidopsis*. *Plant Cell*. 2014;26(4):1544–1556. <https://doi.org/10.1105/tpc.114.122986>
- Xu XF, Wang B, Lou Y, Han WJ, Lu JY, Li DD, Li LG, Zhu J, Yang ZN. Magnesium transporter 5 plays an important role in Mg transport

- for male gametophyte development in *Arabidopsis*. *Plant J.* 2015;84(5):925–936. <https://doi.org/10.1111/tpj.13054>
- Xue JS, Zhang B, Zhan H, Lv YL, Jia XL, Wang T, Yang NY, Lou YX, Zhang ZB, Hu WJ, et al. Phenylpropanoid derivatives are essential components of sporopollenin in vascular plants. *Mol Plant.* 2020;13(11):1644–1653. <https://doi.org/10.1016/j.molp.2020.08.005>
- Yang C, Vizcay-Barrena G, Conner K, Wilson ZA. MALE STERILITY1 is required for tapetal development and pollen wall biosynthesis. *Plant Cell.* 2007;19(11):3530–3548. <https://doi.org/10.1105/tpc.107.054981>
- Yang J, Tian L, Sun MX, Huang XY, Zhu J, Guan YF, Jia QS, Yang ZN. AUXIN RESPONSE FACTOR17 is essential for pollen wall pattern formation in *Arabidopsis*. *Plant Physiol.* 2013;162(2):720–731. <https://doi.org/10.1104/pp.113.214940>
- Zhang W, Sun Y, Timofejeva L, Chen C, Grossniklaus U, Ma H. Regulation of *Arabidopsis* tapetum development and function by DYSFUNCTIONAL TAPETUM1 (DYT1) encoding a putative bHLH transcription factor. *Development.* 2006;133(16):3085–3095. <https://doi.org/10.1242/dev.02463>
- Zhang ZB, Zhu J, Gao JF, Wang C, Li H, Li H, Zhang HQ, Zhang S, Wang DM, Wang QX, et al. Transcription factor AtMYB103 is required for anther development by regulating tapetum development, callose dissolution and exine formation in *Arabidopsis*. *Plant J.* 2007;52(3):528–538. <https://doi.org/10.1111/j.1365-313X.2007.03254.x>
- Zhao D, Li Y, Zhang Z, Xu T, Ye C, Shi T, Wang Y. Extraordinary microcarriers derived from spores and pollens. *Mater Horiz.* 2023;10(4):1121–1139. <https://doi.org/10.1039/D2MH01236G>
- Zhu J, Chen H, Li H, Gao JF, Jiang H, Wang C, Guan YF, Yang ZN. Defective in tapetal development and function 1 is essential for anther development and tapetal function for microspore maturation in *Arabidopsis*. *Plant J.* 2008;55(2):266–277. <https://doi.org/10.1111/j.1365-313X.2008.03500.x>
- Zhu J, Lou Y, Shi QS, Zhang S, Zhou WT, Yang J, Zhang C, Yao XZ, Xu T, Liu JL, et al. Slowing development restores the fertility of thermo-sensitive male-sterile plant lines. *Nat Plants.* 2020;6(4):360–367. <https://doi.org/10.1038/s41477-020-0622-6>
- Zhu J, Lou Y, Xu X, Yang ZN. A genetic pathway for tapetum development and function in *Arabidopsis*. *J Integr Plant Biol.* 2011;53(11):892–900. <https://doi.org/10.1111/j.1744-7909.2011.01078.x>